Nano Energy (2013) 2, 116–123

Available online at www.sciencedirect.com

SciVerse ScienceDirect

journal homepage: www.elsevier.com/locate/nanoenergy

RAPID COMMUNICATION

Preparation of amorphous and nanocrystalline sodium tantalum oxide photocatalysts with porous matrix structure for overall water splitting

Harun Tüysüz[a,*], Candace K. Chan[b,*]

[a]Max-Planck-Institut für Kohlenforschung, Kaiser-Wilhelm-Platz 1, 45470 Mülheim an der Ruhr, Germany
[b]Materials Science & Engineering, School for Engineering of Matter, Transport and Energy, 501 E Tyler Mall, ECG 301, Arizona State University, Tempe, AZ, USA

Received 2 July 2012; received in revised form 9 August 2012; accepted 9 August 2012
Available online 23 August 2012

KEYWORDS
Water splitting;
Hydrogen production;
Photocatalyst;
Porous materials;
Nanomaterials;
Sodium tantalum oxide

Summary
Herein, we report the preparation of a series of surfactant-free nanostructured sodium tantalum oxide using $NaTa(OC_3H_7)_6$ as a single precursor. The reaction conditions for the novel synthetic method were optimized and the morphology and crystal structure of the prepared materials were investigated by transmission electron microscopy (TEM), X-ray diffraction (XRD), and X-ray photoelectron spectroscopy (XPS). Condensation and polymerization of $NaTa(OC_3H_7)_6$ under atmospheric pressure gave a porous amorphous structure that could be converted to crystalline $NaTaO_3$ while crystalline $Na_2Ta_2O_6$ nanocrystals with a 25 nm average particle size could be obtained from a hydrothermal method using NH_3 as a base catalyst. In addition, the photocatalytic behaviors of the prepared materials were investigated for overall water splitting into hydrogen and oxygen. Unexpectedly, porous amorphous sodium tantalum oxide showed much better catalytic activity over the crystalline one. The synthesized $Na_2Ta_2O_6$ nanocrystals also indicated promising activity for overall water splitting without any co-catalyst in comparison to bulk $NaTaO_3$.

Introduction

In the last decade, remarkable efforts have been spent on finding alternative renewable energy sources to substitute fossil fuels owing to their harsh effects on global climate change [1–3]. In addition to energy harvesting from piezoelectrics [4] or thermoelectrics, [5] solar energy has gained considerable interest since it has the potential to provide enormous amounts of energy required by the increasing population and economic expansion of the world [6–10]. Solar energy can be transformed directly to electrical energy using a photovoltaic cell or to chemical energy using

*Corresponding authors.
E-mail addresses: tueysuez@kofo.mpg.de (H. Tüysüz), candace.chan@asu.edu (C.K. Chan).

2211-2855/$ - see front matter © 2012 Elsevier Ltd. All rights reserved.
http://dx.doi.org/10.1016/j.nanoen.2012.08.003

a photochemical cell [11]. The production and efficiency of photovoltaic solar cells are gradually growing and will eventually play a larger role in the global energy portfolio [12,13]. On the other hand, since about 90% of the world's current energy usage is in the form of fuels [14] novel approaches and materials should be explored to convert solar energy directly into storable fuels [15,16]. The photoelectrolysis of water directly with sunlight, which produces clean H_2, is a favorable method for reaching this goal [17–20].

Nowadays, there is a plethora of materials and diverse approaches available for electrochemical [21,22] and photo-chemical water splitting into H_2 and O_2 [23–26]. Powdered or slurry photocatalyst systems are still one of the most attractive means since they have a wide range of benefits and uses on a large-scale. Among powdered photocatalysts, tantalum oxide compounds have displayed encouraging stability and catalytic activity for overall water splitting. Researchers have prepared many tantalates that show high activities for photocatalytic water splitting under UV light irradiation such as $Y_2Ta_2O_2N_2$ [27] $ATaO_3$ (A: Li, Na, and K) [28–30], ATa_2O_6 (A: Ca, Sr, and Ba) [31] $A_2Ta_2O_6$ (A=Na, K) and $CaTa_2O_6$ [32] and $Sr_2Ta_2O_7$ [9]. In particular, $NaTaO_3$ with a perovskite structure is the most active among the tantalates. Kudo and co-workers reported a maximum apparent quantum yield of 56% at 270 nm for $NiO/NaTaO_3$ doped with lanthanum ions, the highest ever reported. The high photocatalytic activity was attributed to the small particle size and the ordered surface nanostep structure of the $NiO/NaTaO_3$:La photocatalyst [33].

As a result, there has been much interest in studying the effect of crystallinity, particle size, structure and morphology of these materials, which could highly affect their photocatalytic activity. In addition, porous films have been shown to display higher photocatalytic activity compared to nonporous films due to the shortened distance between the sites where charge carriers are generated and the interface with the electrolyte [34]. Many studies have identified that the structural features of the perovskite tantalates, such as alkali ion type [29,30], Ta–O–Ta bond angle [35] as well as particle size and surface area [36,37] have a large effect on the hydrogen production rate. These can be tuned in part by changing the synthesis methods. Solid-state [33], sol–gel [35] and hydrothermal routes [38,39] have been explored for controlling the morphology, crystal structure, size, and shape of $NaTaO_3$ photocatalysts.

It has been commonly accepted that highly crystalline materials are required for high photocatalytic activity, since photoexcited electron–hole pairs can recombine at defects. Studies comparing amorphous photocatalysts to their crystalline counterparts have usually found negligible photocatalytic activity in the amorphous forms [30,40]. It is also commonly acknowledged that a large surface area photocatalyst is desired, since it can promote substrate adsorption to the surface and increase the number of active sites for catalysis. However, a tradeoff often occurs, since synthesis methods to obtain highly crystalline materials usually use high temperature treatment, which can often increase the particle size and decrease the surface area. Thus, both high crystallinity and high surface area usually cannot be obtained in the same synthesis.

Despite this conventional wisdom, there have been many recent reports on the study of photocatalytic activity in amorphous materials. For example, mixed amorphous and nanocrystalline TiO_2 powders, or entirely amorphous TiO_2, have been shown to have higher photocatalytic activity for dye degradation than crystalline TiO_2 [34,41,42]. An amorphous surface layer on TiO_2 has been attributed to a change in the electronic structure and bandgap, resulting in improved photocatalytic activity under visible light absorption [43]. Amorphous co-catalyst nanoparticles have also been shown to be highly active and stable [44–48] with amorphous molybdenum sulfide films displaying one of the highest activities for hydrogen evolution amongst non-precious metal catalysts [49]. These studies indicate that nanoscale amorphous materials may have unique catalytic properties compared to their crystalline forms. From a commercial and technological standpoint, if amorphous materials can be designed to have comparable or even higher photocatalytic activities than crystalline or nanocrystalline counterparts, there could be a significant savings in cost and effort, since amorphous materials can be made using low temperature methods. However, a systematic study of amorphous vs. crystalline nanoparticles for overall water-splitting has not been attempted. To this end, we have synthesized and characterized a series of sodium tantalum oxide photocatalysts to serve as model systems to better evaluate the role of crystallinity, particle size, and morphology on photocatalytic water splitting.

Experimental procedure

Porous amorphous sodium tantalum oxide was prepared by simple stirring of 15 mL of 1% wt/v of sodium tantalum isopropoxide {$NaTa(OC_3H_7)_6$, Chemsols} in isopropanol at 70 °C for 24 h. The white precipitate product was centrifuged and washed several times with ethanol and dried in a vacuum oven at 100 °C overnight. $Na_2Ta_2O_6$ nanocrystals were prepared by a hydrothermal route. In a typical synthesis, 4 mL of concentrated (14.8 M) ammonium hydroxide solution (EMD) was added dropwise to 21 mL of 1% wt/v of sodium tantalum isopropoxide {$NaTa(OC_3H_7)_6$, Chemsols} in isopropanol and stirred at room temperature for 15 min. Afterwards, the milky suspension was transferred to a 40 mL Teflon-lined stainless autoclave and heated under autogenous pressure at different temperatures for a range of times. The autoclave was naturally cooled down to room temperature. Then, the white precipitate was centrifuged, followed by washing several times with de-ionized water and absolute ethanol and finally drying at 100 °C overnight. Bulk $NaTaO_3$ and $Na_2Ta_2O_6$ were prepared according to the literature [32,33].

The photocatalytic activity of the prepared materials for water splitting was investigated as following: 10 mg of sample was dispersed in 4 mL of de-ionized water, sonicated for 30 min and then transferred to the reaction cell. Photocatalytic reaction was performed using an outer-irradiation reaction cell connected to an Ar purged, closed gas circulation system. The irradiation was performed at 760 Torr using a 500 W high-pressure (Hg–Xe) lamp (Newport, model 66921) at 100 mW/cm^2. The amount of evolved H_2 and O_2 were determined by using inline gas chromatography (Agilent 3000 MicroGC) using a MS-5A column (GL Sciences) and a TCD detector. Transmission

electron microscopy (TEM) images were taken using a Hitachi H-7650 microscope operating with 120 kV acceleration voltage. Wide angle X-ray diffraction (XRD) measurements were carried out on a Bruker D8 X-ray diffractometer. X-ray photoelectron spectroscopy (XPS) was performed using a PHI 5000 VersaProbe (Physical Electronics) equipped with an Al Kα X-ray radiation source.

Results and discussion

Herein, we synthesized a set of sodium tantalum oxide materials with a variety of morphologies and crystal phases. To optimize the reaction conditions for the preparation of the sodium tantalate nanostructures, we carried out a series of experiments by varying reaction parameters such as temperature, time, solution concentration and pH. We primarily studied hydrolysis and condensation of $NaTa(OC_3H_7)_6$ at temperatures within the range 70–210 °C. When the synthesis was carried out under atmospheric pressure at 70 °C for 24 h, the reaction product consisted of a porous matrix interconnected by short nanowires with a 5 nm average thickness (Figure 1a) and an amorphous structure (Figure 1e).

Since the precursor contains Na and Ta elements, this amorphous structure could be sodium tantalum oxide or tantalum oxide. If sodium is not coordinated in the crystal structure, it would be easily rinsed out during the sample washing step. The material was examined by X-ray photoelectron spectroscopy (XPS) to provide further insight into the composition and the structure. XPS spectra of the amorphous sample (Figure 2) shows a perfect fit to the two Gaussian curve peaks in the range of 29–24 eV which correspond to the Ta ($4f_{5/2}$) and Ta ($4f_{7/2}$) core levels of Ta^{5+} cations located at binding energies of 27.5 and 25.6 eV, respectively. It also shows typical binding energies for sodium (Na_{1s}) in $NaTaO_3$ with a binding energy of 1071.4 eV. These values are in good agreement with the literature [50]. The quantitative XPS analysis result indicated that the molar ratio of Na to Ta was 1.04. This finding confirmed that the amorphous sample is based on sodium tantalum oxide. When this amorphous sample was annealed at a temperature of 600 °C for 3 h, the amorphous structure could be transformed to crystalline $NaTaO_3$ with monoclinic phase (JCPDS 74-2479) as verified by XRD (Figure 1e), which also indicated that the starting amorphous material was based on sodium tantalum oxide. Subsequent to the calcination step, the porous nanostructure shrank and formed large aggregates; however some porosity in the samples were still observed from the TEM micrograph as shown in Figure 1b.

Hydrothermal synthesis is a very effective method for the synthesis of crystalline nanostructured materials. However, when the reaction was performed through the hydrothermal route at 180 °C for 15 and 115 h, the porous amorphous structure was formed once more as seen from TEM micrographs (Figure 1c and d) and XRD patterns (Figure 1e). We did not observe any dramatic change in morphology and crystal structure in the material by increasing the reaction temperature and varying the reaction time.

An acid or base catalyst is commonly used to hydrolyze metal alkoxides to obtain their relevant metal oxides. The relative rate of hydrolysis and condensation reactions, which has an important effect on the morphology and final structures, can be very effectively tuned by varying the pH. To accelerate reaction conditions for the preparation of uniform nanoparticles, we also investigated effects of a base catalyst (ammonia) on the morphology and crystal structure of sodium tantalum oxide at various hydrothermal reaction temperatures and times. TEM images and XRD patterns of the sample series that was prepared in the presence of NH_3 are presented in Figure 3. As seen from the TEM micrographs and XRD pattern in Figure 3a and e, a reaction temperature of 120 °C for 12 h produced a porous amorphous matrix with 3 nm average thicknesses. Increasing the hydrothermal temperature from 120 to 150 °C gave a poorly crystalline $Na_2Ta_2O_6$ porous structure with an average thickness of 6 nm (Figure 3b). Further increasing the reaction temperature and time (180 °C, 20 h) resulted in formation of crystalline $Na_2Ta_2O_6$ consisting of nanoparticles with a size range of 10–25 nm dispersed in the porous structure, indicating a transformation of some of the porous structure to nanoparticles as confirmed by TEM (Figure 3c). Once the temperature was increased to 210 °C, highly crystalline cubic pyrochlore $Na_2Ta_2O_6$ nanoparticles (JCPDS no.: 01-070-1155) with an average particle size of 25 nm were obtained, which indicates complete transformation of the porous matrix structure to a nanoparticle structure (Figure 3d). As shown above, NH_3 plays a key role for the production of crystalline sodium tantalum oxide nanoparticles with pyrochlore structure. Previous studies in ABO_3 materials have shown that the hydroxide concentration is important for obtaining the pyrochlore structure vs. perovskite structure. A higher hydroxide concentration favors the formation of the perovskite structure [51]. The use of ammonia as a mineralizer in hydrothermal synthesis has been shown to favor formation of the pyrochlore structure over the perovskite in other systems [52]. This may be because the ammonia only partially ionizes active hydroxide ions in the solution, which lowers the activity of the hydroxide and allows the formation of a pyrochlore structure.

To determine the optimal reaction time and temperature for the preparation of $Na_2Ta_2O_6$ nanocrystals, a set of samples were also synthesized in the presence of NH_3 base catalyst at 180 °C with a variety of reaction times. TEM micrographs and XRD patterns of samples synthesized at 180 °C for 3, 6, 12 and 24 h are presented in the supporting information Figure S1. After a reaction time of 3 h at 180 °C, the product consisted of a porous matrix with an average wall thickness of 5 nm (Figure S1a), and the XRD pattern of the sample indicates a poorly crystalline structure (Figure S1e). When the reaction time was increased to 6 h, some of the porous matrix transformed into crystalline $Na_2Ta_2O_6$ nanoparticles with an average particle size of 20 nm (Figure S1b). A reaction time of 12 h mostly produced nanoparticles with an average particle size of 26 nm and with better crystallinity. A further increase in reaction time from 12 to 24 h raised the nanoparticle ratio even though a small portion of porous matrix remained in the sample (Figure S1d). After these series of experiments, we can conclude that the optimal reaction temperature and time for the production of crystalline $Na_2Ta_2O_6$ nanoparticles are 210 °C and 12 h, correspondingly.

The photocatalytic activity of porous amorphous $NaTaO_x$ that was prepared at 70 °C (Figure 1a), crystalline $NaTaO_3$ nanocrystals (Figure 1b, obtained by calcination of the

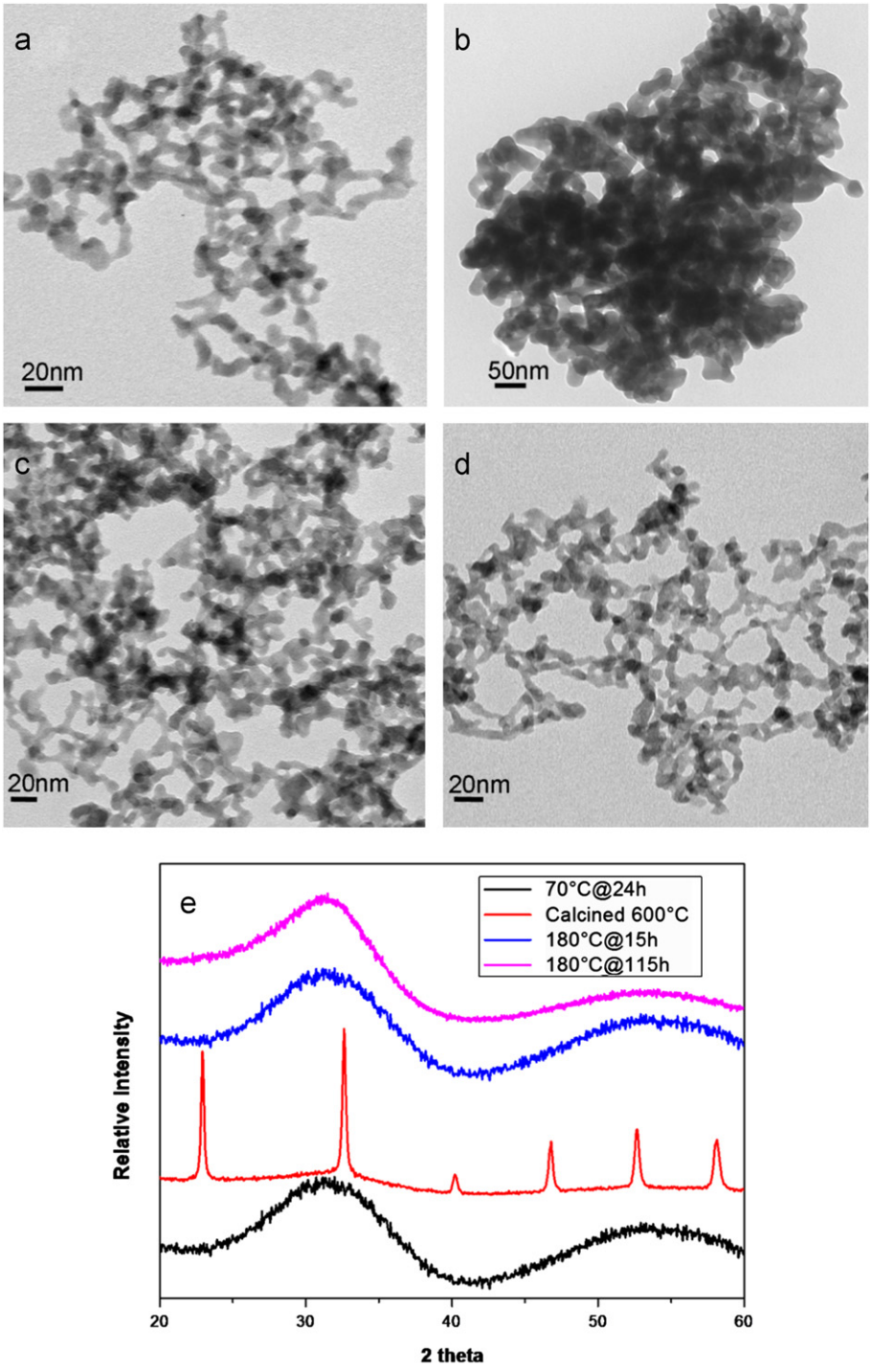

Figure 1 TEM images of (a) amorphous $NaTaO_x$ sample prepared at 70 °C for 24 h, (b) followed by calcination at 600 °C for 3 h to form crystalline $NaTaO_3$. TEM micrographs of sodium tantalum oxide prepared via hydrothermal route at 180 °C for (c) 15 h and (d) 115 h and (e) their XRD patterns.

amorphous $NaTaO_x$ at 600 °C), and $Na_2Ta_2O_6$ nanocrystals (Figure 3c and d) were also evaluated for water splitting. Because reported activities for photocatalysts can vary depending on a number of factors, including reactor design, light intensity, lamp type, and catalyst concentration, we prepared bulk photocatalysts to serve as references using procedures published in the literature. Bulk $NaTaO_3$ was prepared by solid-state reaction of Ta_2O_5 and Na_2CO_3 (labeled as $NaTaO_3$-SS) [33] while $Na_2Ta_2O_6$ was synthesized via hydrothermal route by using $TaCl_5$ and NaOH as starting precursors (labeled as $Na_2Ta_2O_6$-NaOH) [32]. The preparation methods of the samples that were tested as photocatalysts and their activity for overall water splitting are summarized in Table 1. Figure 4 shows the H_2 and O_2 evolved during the irradiation for a set of sodium tantalum oxide photocatalysts.

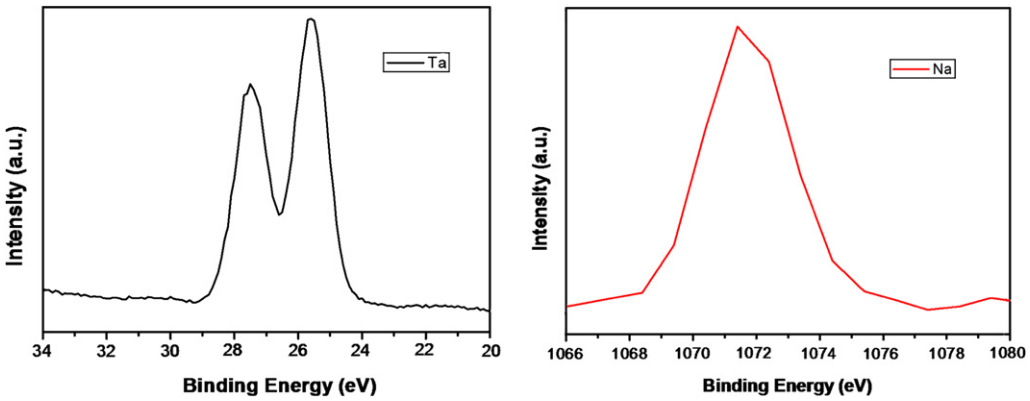

Figure 2 XPS spectra (Ta_{4f} and Na_{1s} peaks) of amorphous sodium tantalum oxide that prepared at 70 °C.

As illustrated in the graph, H_2 and O_2 were evolved in a stoichiometric ratio of approximately 2:1 ratio for all samples. The hydrogen production rate after 2 h for the $NaTaO_3$-SS, amorphous porous $NaTaO_x$, and crystalline $NaTaO_3$ nanocrystals was determined to be 14, 114 and 45 μmol h^{-1} g^{-1}, respectively. The porous amorphous $NaTaO_x$ sample showed an ~8 fold better catalytic activity than $NaTaO_3$-SS. This can be attributed to the smaller particle size and higher surface area of the material, which possesses more active centers that can be involved in the catalytic reaction. Unexpectedly, the crystalline $NaTaO_3$ showed lower catalytic activity in comparison to the amorphous $NaTaO_x$. As mentioned previously, the crystalline $NaTaO_3$ was prepared by calcination of the amorphous $NaTaO_x$ sample using 600 °C. Despite the improvements of crystallinity, which may help to avoid defects and sites where photogenerated electrons and holes can recombine, the thermal treatment also caused the particle size to increase due to sintering and aggregation (Figure 1b), resulting in a decrease in surface area and number of active sites. This indicates that the particle size may play a larger role compared to crystallinity in the activity of photocatalysts, since the photogenerated charge carriers can diffuse to the surface of the particles before recombining more easily in smaller particles. We also note that no co-catalysts were used in these experiments. Co-catalysts such as Pt and NiO for hydrogen evolution can improve charge separation by removing the unfavorable band alignment at the interface between the particle and electrolyte for facile transport of the electrons across the interface. This has shown to be particularly important in wide band-gap oxides such as $NaTaO_3$ in the bulk [33]. However, as the particle size of the material is decreased, the semiconductor becomes fully depleted since the width of the depletion region is on the order of or even larger than the size of the nanoparticle. In this regard, the driving force for charge separation is lost, and the charge carriers must rely on diffusion through the depleted semiconductor to the interface without band bending considerations. As a result, smaller nanoparticles should display improved charge separation, and hence photocatalytic activity for hydrogen production compared to larger nanoparticles. The smaller nanoparticles also have the advantage of a higher surface-to-volume ratio and larger number of active sites on the surface. In our case, we observe that the size consideration is more important than the crystallinity, in contrast to the conventional notion that highly crystalline semiconductors are important for avoiding recombination of charge carriers in photovoltaic and photoelectrochemical applications. This indicates that there are additional advantages to smaller particle-size photocatalysts. Additionally, the observation that the amorphous nanoparticles show higher photocatalytic activity than the bulk and nanocrystalline versions even without co-catalysts may be a promising route for the development of inexpensive yet highly active photocatalysts, since lower temperature methods can be used (since crystallization is not needed) and expensive co-catalysts like Pt are not required.

Although $Na_2Ta_2O_6$ has the same chemical composition with $NaTaO_3$, their photocatalytic activities are different due to their different crystal structures and band gaps [32,33]. $Na_2Ta_2O_6$ nanocrystals with 25 nm average particle size prepared via hydrothermal route using NH_3 as a base catalyst (Figure 3d) and $Na_2Ta_2O_6$-NaOH gave similar H_2 production rates of 87 and 84 μmol h^{-1} g^{-1}, correspondingly. On the other hand, the sample prepared at 180 °C for 20 h consisting of nanoparticles with the interconnected porous matrix structure (Figure 3c) showed a much higher photocatalytic activity by reaching a H_2 production rate of 568 μmol h^{-1} g^{-1}, which is 7 and 40 times higher than that for $Na_2Ta_2O_6$-NaOH and $NaTaO_3$-SS, respectively. This high catalytic activity might be associated with the morphology and/or higher surface area that results from the smaller particle size of the $Na_2Ta_2O_6$. Another possibility is that the band-edge positions of the amorphous matrix and crystalline $Na_2Ta_2O_6$ are slightly different, which can enhance the separation of electron and hole pairs at their interfaces. The separation efficiency of the electron-hole pairs is an important issue that affects the photocatalytic activity of the material. A heterojunction formed between porous amorphous $NaTaO_x$ and crystalline $Na_2Ta_2O_6$ nanoparticles can promote the separation of electron-hole pairs, which increases the photocatalytic performance of the material. A similar observation has also been reported by other researchers who obtained a higher hydrogen evolution rate for a $NaTaO_3/Na_2Ta_2O_6$ composite photocatalyst compared to either $NaTaO_3$ or $Na_2Ta_2O_6$ alone [53]. A comparable phenomenon has been recently seen in a mixture of micro- and nano-sized TiO_2 particles [54] as well, and may also be the case for our mixed porous matrix and nanoparticle morphologies. A further study concerning the higher activity and crystal structure of these materials is in progress.

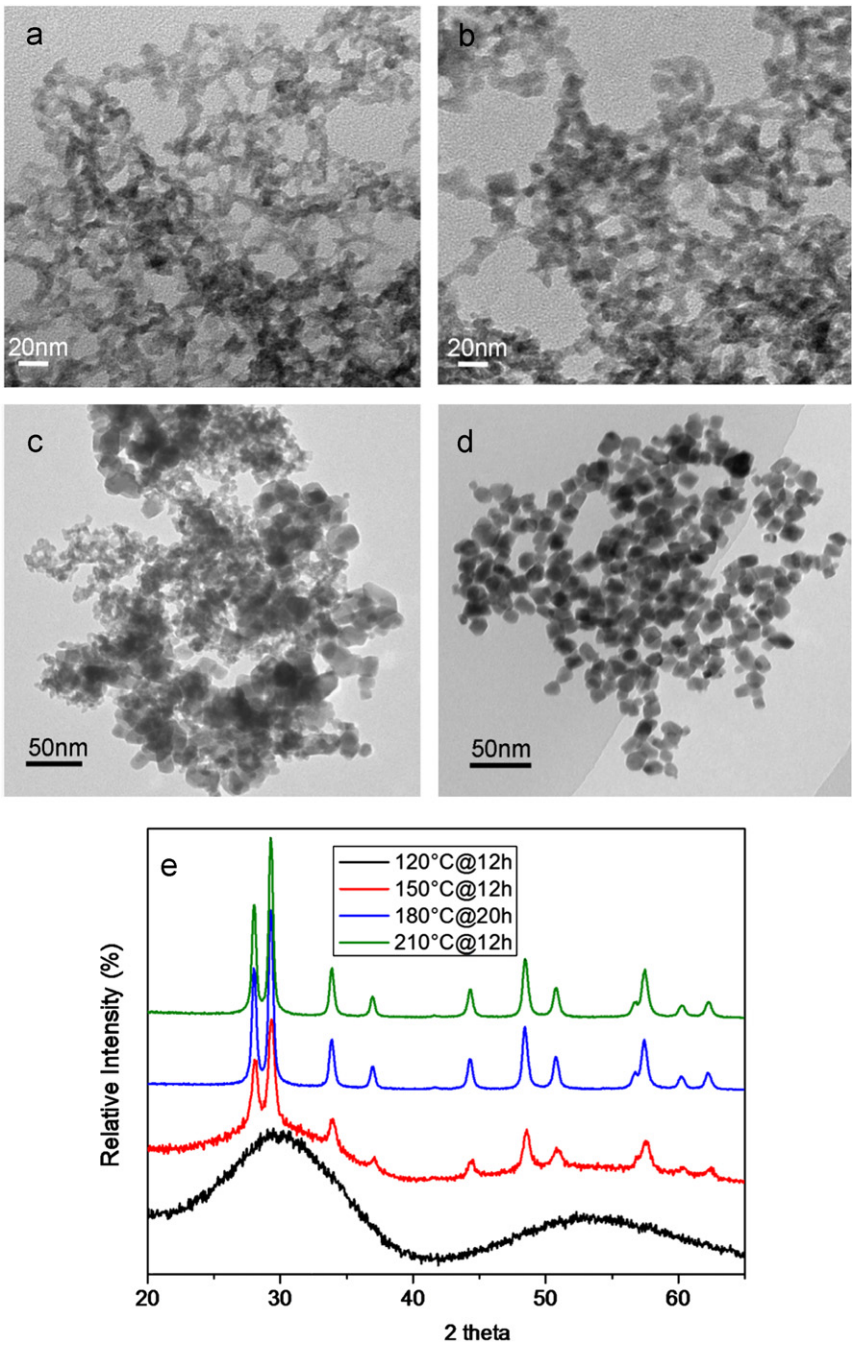

Figure 3 TEM micrographs of sodium tantalum oxide prepared via hydrothermal route at various temperatures in the presence of NH_3, at (a) 120 °C for 12 h, (b) 150 °C for 12 h, (c) 180 °C for 20 h, (d) and 210 °C for 12 h, and their (e) XRD patterns.

Conclusions

In summary, herein we report the synthesis of a set of sodium tantalum oxide materials by using $NaTa(OC_3H_7)_6$ as a single precursor using a wet chemistry technique and hydrothermal route. By precisely controlling the reaction parameters, we could fabricate amorphous porous $NaTaO_x$, crystalline $NaTaO_3$ and crystalline $Na_2Ta_2O_6$ with morphologies that consist of a porous structure with interconnected nanoparticles or nanoparticles only. Our photocatalytic data for overall water splitting confirmed that catalytic activity highly depends on the crystal structure and morphology of the samples, with a maximum catalytic activity obtained for crystalline $Na_2Ta_2O_6$ with a nanoparticle and porous matrix structure. Unpredictably, amorphous porous $NaTaO_x$ indicated better catalytic activity than crystalline $NaTaO_3$. To the best of our knowledge, this is the first report that shows promising catalytic activity in amorphous sodium tantalum oxide for overall water splitting without any co-catalyst, which is a significant step for the fabrication of low-cost semiconductor solid catalysts for water splitting. We believe this strategy can potentially be applied to produce other morphologies, structures and crystal phases of tantalum oxide by further modification of reaction

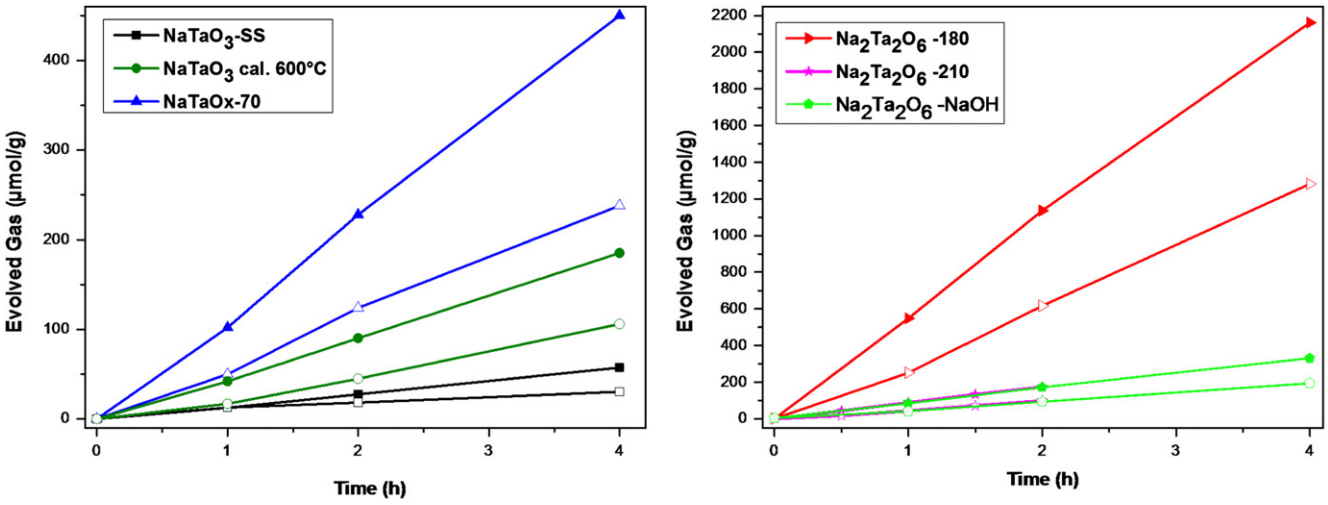

Figure 4 Photocatalytic H_2 (full) and O_2 (empty) evolution over various sodium tantalum oxide samples.

Table 1 The synthesis routes of the samples and their photocatalytic activity for overall water splitting.

Samples	Preparation method	H_2 (μmol g^{-1} h^{-1})	O_2 (μmol g^{-1} h^{-1})
$NaTaO_3$-SS	Solid-solid reaction of Ta_2O_5 with Na_2CO_3 at 1100 °C for 12 h	14	9
$NaTaO_x$	1% wt $NaTa(OC_3H_7)_6$ in iPA, 70 °C 24 h	114	62
$NaTaO_3$-600	$NaTaO_x$ calcined at 600 °C for 3 h	45	22
$Na_2Ta_2O_6$-180	1% wt $NaTa(OC_3H_7)_6$ in iPA-NH_3 solution, 180 °C 20 h, hydrothermal	568	308
$Na_2Ta_2O_6$-210	1% wt $NaTa(OC_3H_7)_6$ in iPA-NH_3 solution, 210 °C 12 h, hydrothermal	87	49
$Na_2Ta_2O_6$-NaOH	$TaCl_5$ in acetylacetone/aqueous NaOH, 140 °C 12 h, hydrothermal	84	45

conditions to improve photocatalytic performance of the material. A further study regarding the photocatalytic activity of amorphous sodium tantalum oxide with a range of morphologies is in progress.

Acknowledgments

H. Tüysüz and C. K. Chan would like to acknowledge the German Research Foundation (DFG) and Miller Institute for Basic Research for their funding, as well as Prof. Peidong Yang for his support and discussion.

Appendix A. Supporting information

Supplementary data associated with this article can be found in the online version at http://dx.doi.org/10.1016/j.nanoen.2012.08.003.

References

[1] P.V. Kamat, Journal of Physical Chemistry C 111 (2007) 2834.
[2] M.E. Himmel, S.Y. Ding, D.K. Johnson, W.S. Adney, M.R. Nimlos, J.W. Brady, T.D. Foust, Science (New York, NY) 315 (2007) 804.
[3] M.S. Dresselhaus, I.L. Thomas, Nature 414 (2001) 332.
[4] W. Xudong, Nano Energy 1 (2012) 13.
[5] W. Liu, X. Yan, G. Chen, Z. Ren, Nano Energy 1 (2012) 42.
[6] R.M.N. Yerga, M.C.C. Galvan, F. del Valle, J.A. Viloria de la Mano, J.L.G. Fierro, ChemSusChem 2 (2009) 471.
[7] S. Ikeda, T. Takata, T. Kondo, G. Hitoki, M. Hara, J.N. Kondo, K. Domen, H. Hosono, H. Kawazoe, A. Tanaka, Journal of the Chemical Society, Chemical Communications (1998) 2185.
[8] O. Khaselev, J.A. Turner, Science (New York, NY) 280 (1998) 425.
[9] A. Kudo, H. Kato, S. Nakagawa, The Journal of Physical Chemistry B 104 (2000) 571.
[10] J.H Yuma, S-J Moona, C.S. Karthikeyan, H. Wietasch, M. Thelakkat, S.M. Zakeeruddin, M.K. Nazeeruddin, M. Gratzel, Nano Energy 1 (2012) 6.
[11] A. Kudo, Y. Miseke, Chemical Society Reviews 38 (2009) 253.
[12] A.J. Frank, N. Kopidakis, J. van de Lagemaat, Coordination Chemistry Reviews 248 (2004) 1165.
[13] M. Law, L.E. Greene, J.J. Cohnson, R. Saykally, P.D. Yang, Nature Materials 4 (2005) 455.
[14] BP Statistical Review of World Energy, 〈http://www.bp.com〉, 2011.
[15] M. Woodhouse, B.A. Parkinson, Chemical Society Reviews 38 (2009) 197.
[16] R. Yu, Q. Lin, S.F. Leung, Z. Fan, Nano Energy 1 (2012) 57.
[17] X. Chen, S. Shen, L. Guo, S.S. Mao, Chemical Reviews 110 (2010) 6503.
[18] R.M. Navarro, M.C. Sanchez-Sanchez, M.C. Alvarez-Galvan, F. del Valle, J.L.G. Fierro, Energy & Environmental Science 2 (2009) 35.
[19] R. van de Krol, Y. Liang, J. Schoonman, Journal of Materials Chemistry 18 (2008) 2311.
[20] X. Zong, H. Yan, G. Wu, G. Ma, F. Wen, L. Wang, C. Li, Journal of the American Chemical Society 130 (2008) 7176.
[21] J. Rossmeisl, Z.W. Qu, H. Zhu, G.J. Kroes, J.K. Norskov, Journal of Electroanalytical Chemistry 607 (2007) 83.
[22] A.J. Esswein, M.J. McMurdo, P.N. Ross, A.T. Bell, T.D. Tilley, Journal of Physical Chemistry C 113 (2009) 15068.

[23] F.E. Osterloh, Chemistry of Materials: A Publication of the American Chemical Society 20 (2008) 35.
[24] A. Paracchino, V. Laporte, K. Sivula, M. Grätzel, E. Thimsen, Nature Materials 10 (2011) 456.
[25] R.K. Hocking, R. Brimblecombe, L.Y Chang, A. Singh, M.H. Cheah, C. Glover, W.H. Casey, L. Spiccia, Nature Chemistry 3 (2011) 461.
[26] Z.G. Zou, J.H. Ye, K. Sayama, H. Arakawa, Nature 414 (2001) 625.
[27] M. Liu, W. You, Z. Lei, G Zhou, J. Yang, G. Wu, G. Ma, G. Luan, T. Takata, M. Hara, K. Domen, C. Li, Chemical Communications 19 (2004) 2192.
[28] H. Kato, A. Kudo, Journal of Photochemistry and Photobiology A: Chemistry 145 (2001) 129.
[29] H. Kato, A. Kudo, The Journal of Physical Chemistry B 105 (2001) 4285.
[30] H. Kato, A. Kudo, Catalysis Today 78 (2003) 561.
[31] H. Kato, A. Kudo, Chemical Physics Letters 295 (1998) 487.
[32] S. Ikeda, M. Fubuki, Y.K. Takahara, M. Matsumura, Applied Catalysis A: General 300 (2006) 186.
[33] H. Kato, K. Asakura, A. Kudo, Journal of the American Chemical Society 125 (2003) 3082.
[34] L. Zhang, X. Li, Z. Mou, S. Wang, F. He, Materials Letters 63 (2009) 165.
[35] C.C. Hu, H. Teng, Applied Catalysis A: General 331 (2007) 44.
[36] Y. Lee, T. Watanabe, T. Takata, M. Hara, M. Yoshimura, K. Domen, Bulletin of the Chemical Society of Japan 80 (2007) 423.
[37] W.H. Lin, C. Cheng, Applied Physics Letters 89 (2006) 211904.
[38] X. Li, J. Zang, Journal of Physical Chemistry C 113 (2009) 19411.
[39] X. Li, J. Zang, Catalysis Communications 12 (2011) 1380.
[40] B. Ohtani, Y. Ogawa, S. Nishimoto, The Journal of Physical Chemistry B 101 (1997) 3746.
[41] S. Buddee, S. Wongnawa, U. Sirimahachai, W. Puetpaibool, Materials Chemistry and Physics 126 (2011) 167.
[42] J. Zou, J. Gao, F. Xie, Journal of Alloys and Compounds 497 (2010) 420.
[43] X. Chen, L. Liu, P.Y. Yu, S.S. Mao, Science (New York, NY) 331 (2011) 746.
[44] M.L. Tang, D.C. Grauer, B. Lassalle-Kaiser, V.K. Yachandra, L. Amirav, J.R. Long, J. Yano, A.P. Alivisatos, Angewandte Chemie International Edition 50 (2011) 10203.
[45] A Minguzzi, F.R.F. Fan, A. Vertova, S. Rondinini, A.J. Bard, Chemical Science 3 (2012) 217.
[46] E. Navarro-Flores, Z.W. Chong, S. Omanovic, Journal of Molecular Catalysis A: Chemical 226 (2005) 179.
[47] M.W. Kanan, D.G. Nocera, Science (New York, NY) 321 (2008) 1072.
[48] X. Li, F.C. Walsh, D. Pletcher, Physical Chemistry Chemical Physics 13 (2011) 1162.
[49] D. Merki, S. Fierro, H. Vrubel, X. Hu, Chemical Science 2 (2011) 1262.
[50] J.P. Schreckenbach, K. Witke, D. Butte, G. Marx, Fresenius' Journal of Analytical Chemistry 363 (1999) 211.
[51] G.K.L. Goh, S.M. Haile, C.G. Levi, F.F. Lang, Journal of Materials Research 17 (2002) 3168.
[52] G. Xu, W. He, Y. Zhao, Y. Liu, Z. Ren, G. Shen, G. Han, CrystEngComm 13 (2011) 1498.
[53] L. Huang, Q. Chan, B. Zhang, X. Wu, P. Gao, Z. Jiao, Y. Lui, Chinese Journal of Catalysis 32 (2011) 1822.
[54] T.Y. Ke, C.Y. Lee, H.T. Chiu, Applied Catalysis A: General 381 (2010) 109.

Harun Tüysüz received his Ph.D. in chemistry from the Max-Planck-Institut für Kohlenforschung in 2008 under the supervision of Prof. Ferdi Schüth. He was awarded a research fellowship from the DFG and did his postdoctoral work at the University of California at Berkeley. Since 2012, he is a group leader at the Max-Planck-Institut für Kohlenforschung. His research interests include heterogeneous catalysis and sustainable energy, shape controlled nanocrystals and design of multi-functional ordered mesoporous polymer and metal oxides.

Candace K. Chan received her B.S. in chemistry in 2005 from Rice University, where she worked in the lab of Prof. R.E. Smalley. She joined Prof. Y. Cui's group at Stanford University and received her Ph.D. in physical chemistry from Stanford in 2009. After a postdoc as a Miller Fellow at the University of California at Berkeley, in 2011 she joined Arizona State University as an Assistant Professor in the Materials Science and Engineering program in the School for Engineering of Matter, Transport and Energy. Her research interests include the synthesis and evaluation of nanomaterials for energy storage and photoelectrochemical applications.